

Measurement of the dependence of the light yields of linear alkylbenzene-based and EJ-301 scintillators on electron energy

H. Wan Chan Tseung*, J. Kaspar, N. Tolich

Center for Experimental Nuclear Physics and Astrophysics, and Department of Physics, University of Washington, Seattle, WA 98195

Abstract

An experimental test of the electron energy scale linearities of SNO+ and EJ-301 scintillators was carried out using a Compton spectrometer with electrons in the energy range 0.09–3 MeV. The linearity of the apparatus was explicitly demonstrated. It was found that the response of both types of scintillators with respect to electrons becomes non-linear below ~ 0.4 MeV. An explanation is given in terms of Cherenkov light absorption and re-emission by the scintillators.

Keywords: scintillator, linearity, energy scale, linear alkylbenzene, SNO+

1. Introduction

SNO+ is a multi-purpose neutrino experiment whose reach extends to the following areas of neutrino physics: neutrinoless double beta decay (with Nd-loaded scintillator), geo-neutrinos, reactor and low-energy solar neutrinos, as well as supernova neutrinos [1]. It is a ~ 780 -tonne liquid scintillator (LS) detector currently under construction ~ 2 km underground at the SNOLAB facility in Sudbury, Ontario, Canada. The scintillator will be contained in a 12-m diameter spherical acrylic vessel surrounded by ~ 9500 photomultiplier tubes (PMTs). More details on the layout can be found in [2].

The LS to be used in SNO+ is linear alkylbenzene (LAB) with ~ 2 g/L of PPO (2,5-diphenyloxazole). In the double-beta decay phase, the LAB-PPO will be loaded with ~ 0.1 % Nd (by weight). To achieve the goals of the experiment, it is imperative to understand the properties of this scintillator down to the SNO+ energy threshold, which is expected to be ~ 0.2 MeV for low-energy solar neutrino studies. In particular, for electrons, a precise knowledge of the dependence of the light yield, \mathcal{L} , on their kinetic energy, E_e , is required. For scintillators, $\mathcal{L}(E_e)$ is commonly assumed to be linear, except at very low energies (typically below ~ 50 keV), where the effects of ionization quenching appear to be important. The decrease in light yield due to ionization quenching is well-described for all particles by Birks' law [3].

In the last decade, the KamLAND experiment observed, using γ -ray calibration sources, that the electron energy scale of a dodecane-based scintillator was non-linear and could not be solely described by Birks' law [4]. A laboratory investigation of the KamLAND LS electron energy scale with a Compton spectrometer confirmed these results [5]. It was hypothesized that Cherenkov light, being absorbed and re-emitted by the LS, acted as another scintillation light 'source' besides ionization. This led to a rise in $d\mathcal{L}/dE_e$ in the energy region above the Cherenkov threshold for electrons.

The primary aim of this work is to test the linearity of $\mathcal{L}(E_e)$ for both LAB-PPO and Nd-doped LAB-PPO, in an energy range relevant to the various goals of the SNO+ experiment, *i.e.* up to 3.5 MeV. We verify if the SNO+ LS displays the same behaviour as KamLAND's, and quantify the extent of the Cherenkov contribution to non-linearity. We also test the linearity of EJ-301 scintillator [6], which is equivalent to the commonly-used NE-213. Details of our apparatus and method are given in §2. §3 describes a measurement of the non-linearity of our set-up. The results of our scintillator linearity tests are presented and discussed in §4. We summarize and conclude in §5.

2. Experimental method

To measure the scintillation light output as a function of E_e , we used the Compton scattering of γ -rays of known energies, E_γ , to produce mono-energetic elec-

*Corresponding author. Tel: +1 206 543 4035; fax: +1 206 685 4634. Email address: hwan@uw.edu

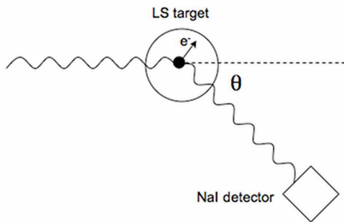
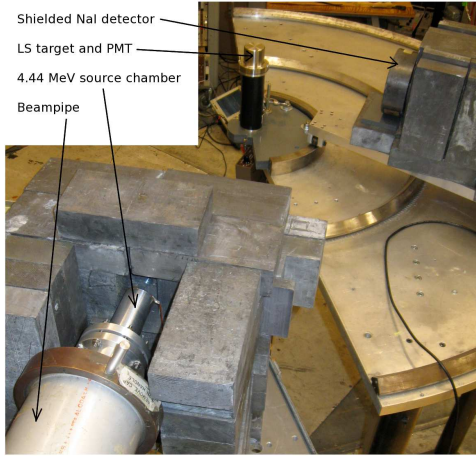


Figure 1: Set-up of the apparatus.

trons within the LS. E_e is given by:

$$E_e = E_\gamma - E'_\gamma \quad (1)$$

where E'_γ is the scattered γ energy. E'_γ is calculated using the Compton formula:

$$E'_\gamma = \frac{E_\gamma}{1 + \frac{E_\gamma}{m_e c^2} (1 - \cos \theta)} \quad (2)$$

where m_e is the electron mass, and θ is the γ scattering angle (defined in the lower part of fig. 1). The scattered γ was recorded with a NaI detector placed at angle θ . Only events that resulted in coincident pulses from the LS and NaI detectors were considered. Two γ -ray sources of 0.662 and 4.44 MeV allowed values of E_e in the range 0.09–3 MeV to be probed with high granularity.

Fig. 1 is a photograph of the spectrometer set-up, with the LS cell located 1.5 m from the γ source, and a 2'' NaI detector placed on a trolley with a 0.5-m rotation radius. The γ -rays were collimated by a 5-mm diameter hole drilled through 20 cm of lead shielding. The 0.662 MeV γ s originated from a ^{137}Cs source that was small enough to fit into the collimator hole. The 4.44 MeV source is described below.

2.1. A 4.44 MeV γ -ray source

We constructed a high intensity 4.44 MeV γ source using the $^{12}\text{C}(p,p')^{12}\text{C}$ reaction. A $\sim 2 \mu\text{A}$ 5.7 MeV proton beam was supplied by the CENPA tandem Van de Graaff accelerator. Our source chamber, seen in fig. 1, was made of aluminium. It consisted of a flange reducer section that interfaced to the beam pipe, and an insulated target holder section connected to a pico-ammeter for flux monitoring. A small tantalum aperture located at the beam pipe interface ensured that most γ s were produced at the centre of the carbon target, which was a 5-mm thick disk of natural carbon. Cooling for the latter was not required. We carefully aligned the LS cell, γ -ray collimator, and the proton beam collimating and focussing apertures with a surveying telescope located far away in the 0° direction.

The $^{12}\text{C}(p,p')^{12}\text{C}$ cross-section was previously measured by Barnard *et al.* and Dyer *et al.* [7, 8]. The beam was operated at 5.7 MeV to select the first resonance peak and reduce backscattered γ backgrounds in the experimental hall as much as possible. At $2 \mu\text{A}$ of 5.7 MeV proton beam current, and assuming a cross-section of 200 mb, we estimated the overall source strength to be a few tens of mCi.

A NaI detector placed along the beamline and 2 m from the Carbon target, confirmed the intense 4.44 MeV gamma event rate. Two other photons, with energies of 3.11 and 0.511 MeV, were emitted from $^{13}\text{C}(p,p')^{13}\text{C}$, and from the decay of ^{13}N produced in the $^{13}\text{C}(p,n)^{13}\text{N}$ reaction. The relative contributions of the 4.44, 3.11 and 0.511 MeV γ s are 89.1, 0.9 and 10%, respectively [9]. At any angle θ , the values of E_e for recoil electrons in the LS from the 0.511 MeV and 4.44 MeV γ s were very different, while the 3.11 MeV γ interfered with the electron signal from the 4.44 MeV line at the $< 1\%$ level. Therefore, the 0.511 and 3.11 MeV lines can be neglected in this work.

2.2. Scintillator cell

Two scintillator-PMT assemblies were custom-designed and built with all materials in direct contact with the active volume being compatible with the LAB-based and EJ-301 scintillators. The scintillator was coupled to a Philips Valvo XP-2262 PMT, housed in mu-metal shielding, via a pyrex window. The PMT was biased to -1400 V. The 2'' \times 2'' cylindrical scintillator container was bored out of a solid piece of stainless steel. Its walls were 1 mm thick, with mirror-polished inner surfaces.

Both of our LAB-based LS samples contained 3 g/L of PPO. Before filling, the LS was de-oxygenated by

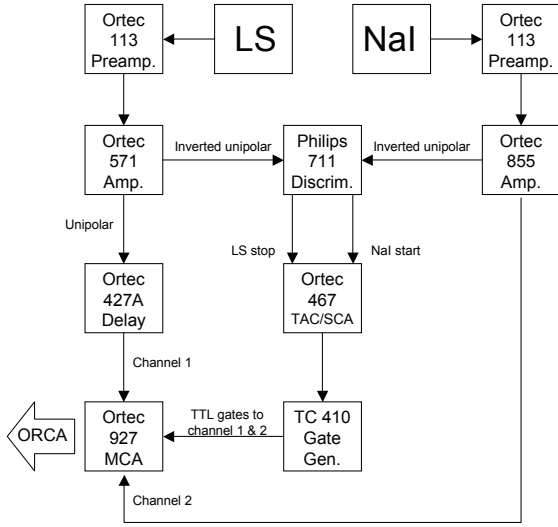


Figure 2: Schematic of the electronics chain.

128 gently bubbling in Ar gas for ~ 45 minutes [10]. The
 129 cells were cleaned in an ultra-sound bath, before being
 130 vacuum-filled with the LS. We used tubes and valves
 131 that were made entirely of teflon.

132 2.3. Electronics and data acquisition

133 An NIM-based electronics set-up (shown in fig. 2)
 134 recorded the charge of coincident PMT pulses from the
 135 NaI and liquid scintillator detectors. The pulse height
 136 spectra from the multi-channel analyzer (MCA) were
 137 read in by ORCA, a data-acquisition software developed
 138 at the Universities of Washington and North Carolina
 139 [11].

140 2.4. Data-taking procedure

141 The electronics and PMT were allowed to stabilize
 142 overnight before data-taking the next day. To avoid
 143 making corrections due to gain drifts, measurements
 144 with the 4.44 MeV and 0.662 MeV γ s were done on the
 145 same day, with the ^{137}Cs runs starting soon after switch-
 146 ing off the proton beam. For consistency, the LAB-
 147 PPO and Nd-doped LAB-PPO measurements were per-
 148 formed using the same scintillator cell and the same
 149 PMT, which underwent the linearity tests described in
 150 §3. The electronics settings were fixed throughout the
 151 whole experiment.

152 Fig. 3 shows the LS pulse height spectra at seven an-
 153 gles between 28.5° and 141° . This data was taken with
 154 the ^{137}Cs source and LAB-PPO target. At each angle,

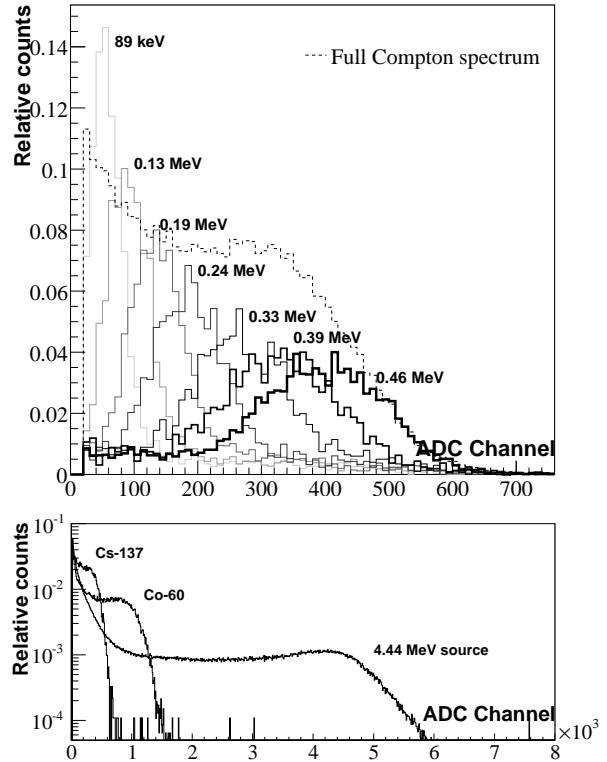


Figure 3: Top: From left to right, the solid-line histograms are the observed electron recoils in LAB-PPO resulting from the 28.5° , 36° , 46° , 56° , 76° , 96° and 141° scattering of γ -rays originating from a ^{137}Cs source. The reconstructed values of E_e at each angle are given. The dotted line is the full Compton scattering spectrum. Bottom: The LAB-PPO Compton spectra of 0.662, ~ 1.25 and 4.44 MeV γ s from ^{137}Cs , ^{60}Co and the $^{12}\text{C}(p,p')^{12}\text{C}$ reaction, respectively.

155 mono-energetic electron peaks can unambiguously be
 156 located to give \mathcal{L} in units of ADC bins. The full Com-
 157 pton spectrum, drawn in dotted line, is shown for com-
 158 parison. The bottom plot shows two more Compton
 159 spectra, obtained with a ^{60}Co source and our 4.44 MeV
 160 accelerator source.

161 3. Linearity of apparatus

162 The recorded ADC peak positions from the LS can
 163 scale non-linearly with E_e for the following reasons:
 164 (1) the scintillator response is intrinsically non-linear,
 165 (2) the integrated charge from the XP-2262 PMT pulses
 166 did not increase linearly with the number of photons in-
 167 cident on its photocathode, (3) the electronics chain dis-
 168 torted the energy scale, and (4) the apparatus was mis-
 169 aligned, resulting in erroneous values of E_e when using
 170 the Compton equation with scattering angles that were

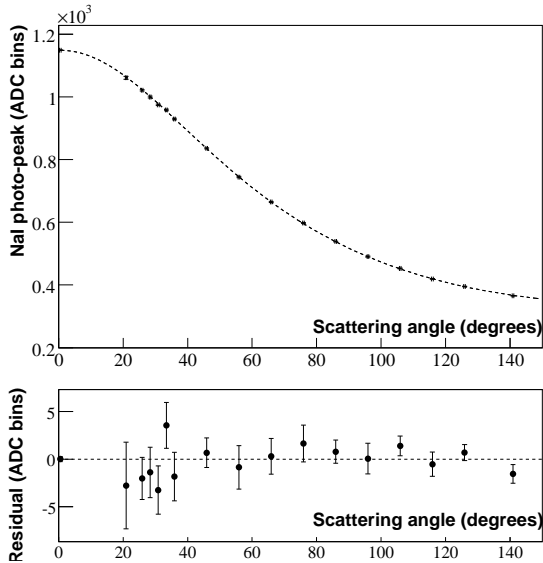


Figure 4: Top: The angular dependence of NaI photo-peak positions (black markers) of γ s from a ^{137}Cs source, scattered off a Nd-doped LAB-PPO target. The dotted line is a fit to Eq. 3. Bottom: Fit residuals.

171 not corrected for this misalignment. The last three issues
172 are discussed below.

173 3.1. Misalignment and electron energy reconstruction

174 The spectrometer misalignment can be studied by fitting
175 the angular dependence of NaI photo-peak positions,
176 $f(E'_\gamma)$, from ^{137}Cs source data to the Compton
177 formula, Eq. 2. The fit function was:

$$178 \quad f(E'_\gamma) = \frac{a \cdot E_\gamma}{1 + \frac{E_\gamma}{m_e c^2} (1 - \cos(\theta + \delta))} + b \quad (3)$$

179 where a and b are constants, and δ is an angular offset
180 to account for the misalignment. Fig. 4 shows NaI data
181 (black markers) fitted to Eq. 3 from 0° to 141° . The un-
182 certainty on reading out θ was estimated to be $\pm 0.25^\circ$.
183 Except at $\theta = 0^\circ$, all the data were collected in coinci-
184 dence with the LS. When δ was fixed to 0° , the χ^2/NDF
185 for the fit was 19.9/15. When it was allowed to float, the
186 best fit value for δ was $-0.36^\circ \pm 0.13^\circ$, with an improved
187 χ^2/NDF of 7.8/14. To account for this angular offset,
188 we increase our uncertainty in the scattering angle from
189 $\pm 0.25^\circ$ to $\pm 0.36^\circ$. The residuals for the unconstrained
190 fit are shown in the lower plot of fig. 4.

191 We performed further checks on the reconstructed E_e
192 values using another method, which consists of calibrat-
193 ing the NaI energy scale with ^{137}Cs , ^{207}Bi and ^{152}Eu
194 γ -ray sources. A fit to a straight line below 0.7 MeV

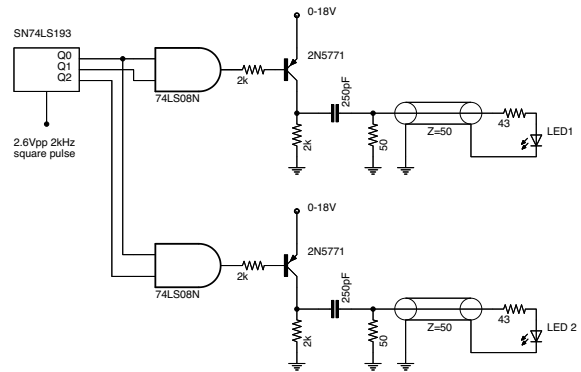


Figure 5: Schematic of the LED driver circuit.

195 yielded values of a and b that were consistent with the
196 Compton fit. The calibration constants were then used
197 to get E'_γ , and hence E_e . This method is independent
198 of the one described in §2, because no assumptions are
199 made about Compton scattering. The mean percentage
200 difference between the values of E_e reconstructed using
201 the two methods was -0.4% for ^{137}Cs data with a LAB-
202 PPO target, and 1% for a Nd-doped LAB-PPO target.

203 Note that the second method is applicable only when
204 the NaI photo-peaks for the scattered γ s are clearly visi-
205 ble. For the 4.44 MeV γ data, this was not the case, and
206 it was assumed Eq. 2 still accurately applied.

207 3.2. Measurement of the linearity of PMT and electron- 208 ics chain

209 For the LAB-based LS, the linearity of the PMT and
210 electronics chain was verified using a system of two se-
211 quentially flashing Light Emitting Diodes (LEDs), fol-
212 lowing the method described in [12]. The two LEDs
213 (diffuse yellow HLMP-3401) were placed adjacent to
214 each other, 10 cm in front of the XP-2662 in a light-tight
215 box. The PMT was connected to exactly the same elec-
216 tronics (with the same voltage and gain settings) as in
217 the scintillator linearity measurements. An LED driver
218 (fig. 5) continuously flashed the LEDs in the following
219 sequence consisting of three steps: (A) LED 1 only, (B)
220 LED 2 only, and (C) LEDs 1 and 2 at the same time. The
221 driver circuit consisted of a 4-bit binary counter driven
222 by an Agilent 33120a pulser. The Q_0 , Q_1 and Q_2
223 outputs from the counter were fed to two AND gates as
224 shown in fig. 5. The logic outputs operated PNP tran-
225 sistor switches that were capacitively coupled to LEDs
226 1 and 2. The resulting pulses were 20 ns wide at full-
227 width-half-maximum, with a variable amplitude of 0–4
228 V. The pulse amplitudes, and thus the number of pho-
229 tons incident on the PMT, were controlled by an Instek

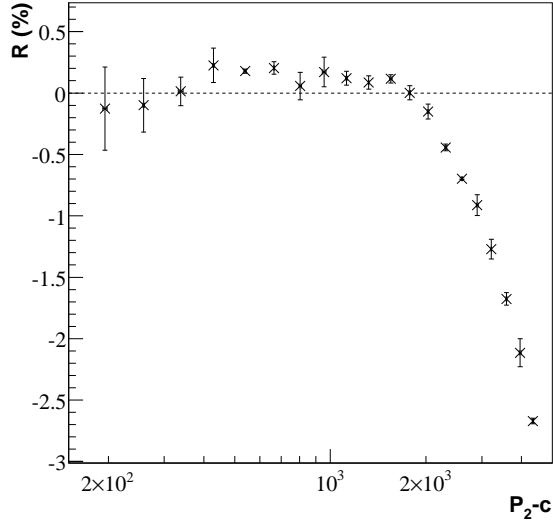


Figure 6: Measured non-linearity of the PMT and electronics chain. The PMT that underwent the test was the one used in the LAB-based scintillator measurements.

GPS-3303 DC power supply, which biased the emitters of the two transistor switches. To reduce reflections, a 43 Ω resistor was placed in series with the LEDs, which had a forward bias resistance of $\sim 6 \Omega$.

The voltage pulses during steps A and C, as well as B and C were observed to be nearly identical. The following ratio R quantifies non-linearity:

$$R = 100 \cdot \frac{(P_3 - P_1) - P_2 + c}{P_2 - c} \quad (4)$$

where P_1 , P_2 and P_3 are the ADC peak positions in steps A, B and C respectively, and c is the pedestal in number of ADC channels. The power supply voltages to the two transistors were varied such that $P_1 < P_2$ and $P_1/P_3 \approx 1/3$ and $P_2/P_3 \approx 2/3$. Fig. 6 shows R as a function of $P_2 - c$. The difference between P_3 and P_1 is consistent with P_2 at the 0.2% level, except at high ADC channels, when space charge effects in the PMT become important. The resulting gain loss makes P_3 lower than $P_1 + P_2$. We will discuss our results in terms of the non-linearity parameter R in the next section.

c was measured by injecting an exponentially-decaying pulse of controllable amplitude into the Ortec 571 amplifier (fig. 2). It was found to be -10.72 ± 0.73 . In the process of measuring c , we confirmed the linearities of the Ortec 571 amplifier, 427A delay and 927 MCA units that were used to record pulse heights from the LS PMT.

4. Results

Our measurements of $\mathcal{L}(E_e)$ in ADC counts, for LAB-PPO (26 data points), Nd-doped LAB-PPO (29 data points) and EJ-301 (18 data points), are shown in cross markers in figs. 7(a), (b) and (c), respectively. For the LAB-based scintillators, $d\mathcal{L}/dE_e$, shown in the lower plots, increases by nearly 50 % in the energy range from 0.2 to 1 MeV. The change in $d\mathcal{L}/dE_e$ is less pronounced for EJ-301. In figs. 7(a) and (b), the circle markers are the 0.48, 1.04 and 4.2 MeV Compton edge positions (evaluated at half-height) for γ s from ^{137}Cs , ^{60}Co , and $^{12}\text{C}(p,p')^{12}\text{C}$, respectively. These three data points serve as a further verification of our alignment and energy reconstruction procedure.

In §3.2, we discussed a measurement of the non-linearity R (Eq. 4) due to the PMT and electronics at 15 P_2 values between 200 and 3500 ADC bins. This involved using two light sources (LEDs), one of which was nearly twice as strong as the other. In the LS, the electron is also a light source. For $200 < \mathcal{L}(E_e) < 3500$, we calculated the analogous quantity R' by interpolation:

$$R' = 100 \cdot \frac{\left[\mathcal{L}(E_e) - \mathcal{L}\left(\frac{E_e}{3}\right) \right] - \mathcal{L}\left(\frac{2E_e}{3}\right) + c}{\mathcal{L}\left(\frac{2E_e}{3}\right) - c} \quad (5)$$

If the LS is linear with respect to E_e , R' should be of the same order as R . The insets in figs. 7(a) and (b) show the values of R' as a function of E_e . For both LAB LS samples, these clearly exceed 0.2%, reaching $\sim 20\%$ in the low-energy region. Therefore, the non-linearities seen in figs. 7(a) and (b) were not caused by the PMT and electronics. We assume this to be also the case for fig. 7(c), although R has not been measured for the PMT that was used in the EJ-301 measurements.

4.1. Interpretation and discussion

We now provide a simple model for $\mathcal{L}(E_e)$. At any value of E_e , the total light yield of the LS, in a wavelength region detectable by the PMT, is given by:

$$N_T = N_S + N_C \quad (6)$$

where N_S is the number of photons originating from the scintillation process and N_C is the Cherenkov contribution. N_C includes primary Cherenkov photons, as well as those emitted as a result of LS excitation by Ultra-Violet (UV) Cherenkov photons. $\mathcal{L}(E_e)$ is proportional to N_T . We fitted our data to the following:

$$\mathcal{L}(E_e) = A \cdot N'_S(E_e) + B \cdot N_{C2}(E_e) + C \quad (7)$$

where A and B are scaling constants, and C is an offset. These take into account detector-related effects such as

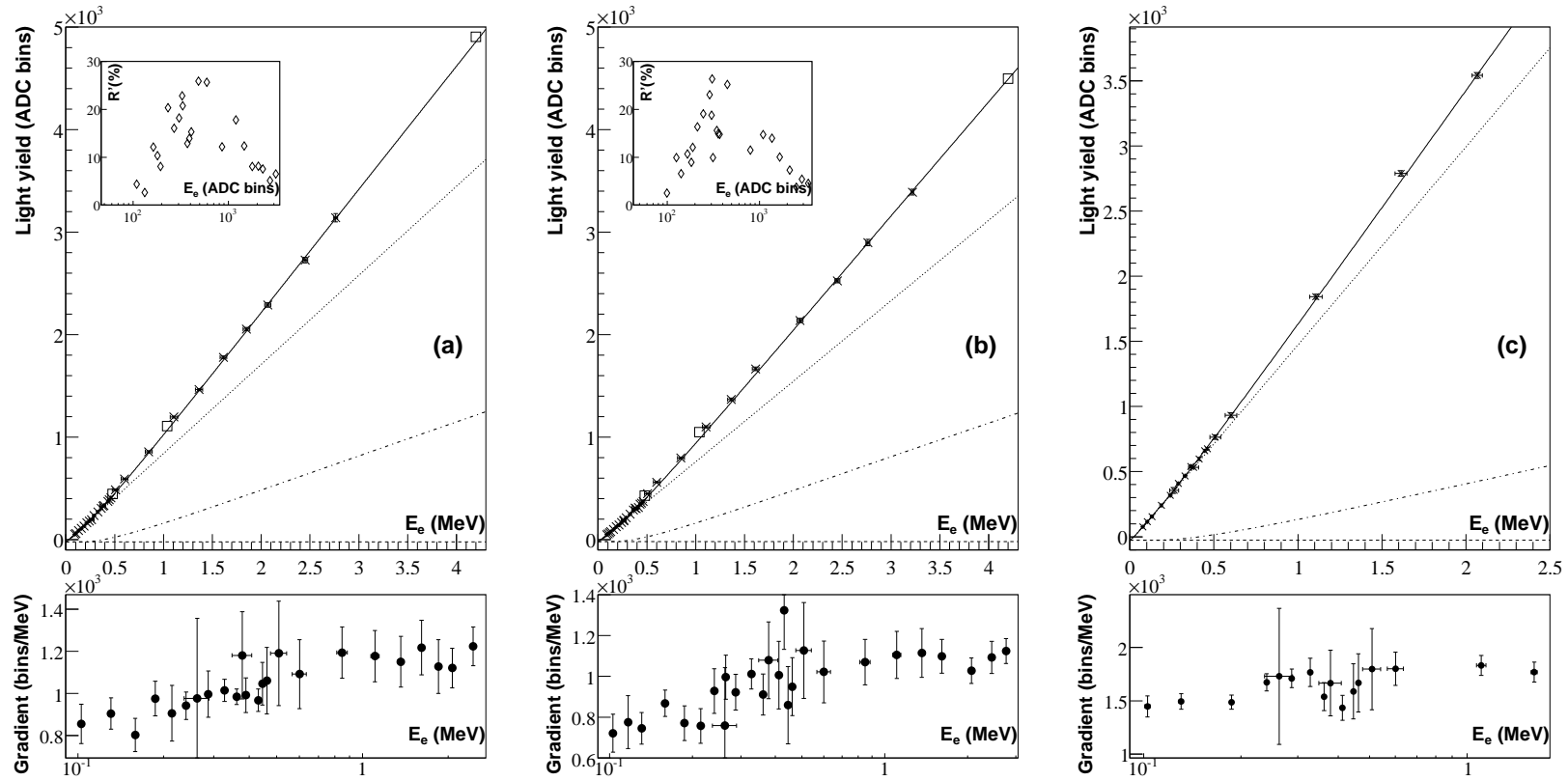


Figure 7: (a) The LAB-PPO, (b) Nd-doped LAB-PPO and (c) EJ-301 electron energy scales $\mathcal{L}(E_e)$ in units of ADC bins. The Compton spectrometer measurements are displayed with the cross markers in the upper plot. The circle markers in (a) and (b) are the Compton edge positions of γ -rays from ^{137}Cs , ^{60}Co , and $^{12}\text{C}(\text{p,p}')^{12}\text{C}$. The solid-line curves are the best fits to a simple light yield model (Eq. 7). The scintillation and Cherenkov components are shown as the dotted and dash-dotted curves, respectively. The lower plots show the change in $d\mathcal{L}/dE_e$ with E_e , while the insets show R' (defined in Eq. 5) as a function of E_e .

301 photon collection and PMT quantum efficiencies, gain, 346
 302 and pedestal. The scintillation component is given by: 347

$$303 \quad A \cdot N'_S = A \cdot \int_{E_e}^0 \frac{1}{1 + k_B S_e(E'_e)} dE'_e \quad (8) \quad 349$$

304 where k_B is Birks' constant, and S_e is the electron stop- 350
 305 ping power, calculated using the ESTAR database [13]. 351
 306 Since the scintillation light yield is unknown, it was fac- 352
 307 tored into A . $N_{C2}(E_e)$ was calculated with: 353

$$308 \quad N_{C2} = \int_{\omega_1}^{\omega_2} \int_{E_e}^{E_f} \frac{\alpha}{S_e(E'_e)} \left(1 - \frac{1}{\beta^2(E'_e) n^2(\omega)} \right) dE'_e d\omega \quad (9) \quad 354$$

309 where β is the electron speed in units of c , and E_f is 355
 310 defined by $\beta(E_f) = 1/n(\omega)$. In Eq. 9, S_e is in units of 356
 311 MeV^2 , the frequency ω and E_e are both in MeV, and the 357
 312 frequency integral is performed over the range 250–800 358
 313 nm. The dispersion $n(\omega)$ comes from our ellipsomet- 359
 314 ric measurements of the refractive indices of SNO+ and 360
 315 EJ-301 LS above 210 nm [14]. The four fit parameters 361
 316 were A , B , C and k_B . Appendix A describes the relation 362
 317 between Eqs. 6 and 7 in more detail. 363

318 The fit results are shown in the upper plots of fig. 7. 364
 319 The scintillation and Cherenkov components are dis- 365
 320 played as the dotted and dash-dotted curves, respec- 366
 321 tively. The solid-line curves show the best fits to the 367
 322 data. For the LAB-PPO sample, the fit returned $A =$ 368
 323 879 ± 12 , $B = 0.78 \pm 0.05$, $C = -23.3 \pm 2.2$, and 369
 324 $k_B \sim 74 \mu\text{m}/\text{MeV}$ with a χ^2/NDF of 12.3/22. In the case 370
 325 of Nd-doped LAB-PPO, $A = 797 \pm 9$, $B = 0.77 \pm 0.03$, 371
 326 $C = -19.3 \pm 1.7$, and $k_B \sim 91 \mu\text{m}/\text{MeV}$ with a χ^2/NDF 372
 327 of 25.7/25. Assuming a scintillation light yield L_S of 373
 328 1×10^4 photons/MeV, it appears that the Cherenkov light 374
 329 yield in the 250–800 nm window, N_{C2} , had to be scaled 375
 330 up by a factor of $L_S B/A \sim 9$ to explain our data. In 376
 331 comparison, we also fitted the data with: 377

$$332 \quad \mathcal{L}(E_e) = A \cdot N'_S(E_e) + C \quad (10) \quad 378$$

333 which assumes a negligible Cherenkov component, and 379
 334 a scintillation light yield governed by Birks' law. The 380
 335 χ^2/NDF for LAB-PPO and Nd-doped LAB-PPO were 381
 336 considerably worse: 264/23 and 492/26, respectively. 382

337 For EJ-301, the results were $A = 1558 \pm 9$, $B = 0.61 \pm$ 383
 338 0.04 , $C = -26.9 \pm 3.5$, and $k_B \sim 161 \mu\text{m}/\text{MeV}$ with a 384
 339 χ^2/NDF of 14.4/14. The χ^2/NDF from the fit to Eq. 10 385
 340 was 51.6/15. 386

341 Therefore, as in the KamLAND case, we find that 387
 342 the non-linearity of the SNO+ LS cannot be accounted 388
 343 for solely by Birks' law for ionization quenching. A 389
 344 combination of quenching and Cherenkov light excita-
 345 tion seems to better describe our measurements. For

346 the SNO+ LS, the dominant contribution to the non-
 347 linearity appears to come from the Cherenkov compo-
 348 nent. This causes an increase in light yield above the
 349 Cherenkov threshold (~ 0.2 MeV).

350 5. Conclusions

351 To summarize, we investigated the dependence of the
 352 light yield on electron energy for EJ-301 and two LAB-
 353 based scintillators with a Compton spectrometer appa-
 354 ratus, whose linear response was verified. The spec-
 355 trometer allowed us to probe a large number of elec-
 356 tron kinetic energy values between 0.09 and 3 MeV. We
 357 found that both LAB scintillator samples demonstrate
 358 an enhancement in the light yield in the vicinity of the
 359 Cherenkov threshold for electrons. This was also ob-
 360 served, albeit to a lesser extent, in the EJ-301 measure-
 361 ments. We provided a simple model to explain these
 362 observations, which deviate from the usual premise of
 363 LS electron energy scale linearity.

364 Acknowledgements

365 This work was supported by the United States De-
 366 partment of Energy grant #DE-FG02-97ER41020. We
 367 thank our Brookhaven National Laboratory collabora-
 368 tors for sending the scintillator samples, M. Chen and
 369 S. Enomoto for helpful discussions, and the CENPA
 370 staff for technical assistance.

371 Appendix A. Cherenkov component

372 Here we show that N_C is directly proportional to
 373 N_{C2} , which is accurately calculable with Eq. 9. Con-
 374 sider the two wavelength ranges: (1) $\lambda < 250$ nm,
 375 where Cherenkov yield cannot be fully calculated be-
 376 cause the refractive index is unknown below 210nm,
 377 and (2) $\lambda > 250$ nm. N_C can be decomposed as:

$$378 \quad N_C = f_{C2} \cdot N_{C2} + f_{C1} \cdot N_{C1} \quad (A.1) \quad 379$$

380 where N_{C1} and N_{C2} are the numbers of Cherenkov pho-
 381 tons in regions 1 and 2, respectively. f_{C1} and f_{C2} are
 382 the fractions that are absorbed in regions 1 and 2, and re-
 383 emitted as one or more photons of longer, detectable,
 384 wavelengths. Since f_{C1} and f_{C2} have not been mea-
 385 sured, and N_{C1} is unknown, it is not possible to perform
 386 an absolute calculation of N_C . However, assuming that
 387 the shape of the Cherenkov spectrum is independent of
 388 electron energy, $(f_{C1} N_{C1} / N_{C2} + f_{C2})$ is constant at all E_e .
 Thus, $N_C \propto N_{C2}$.

389 **References**

- 390 [1] M.C. Chen, The SNO+ Experiment, proceedings of the 34th In-
391 ternational Conference on High Energy Physics (ICHEP 2008),
392 Philadelphia, Pennsylvania (2008). arXiv:0810.369
393 [2] The SNO Collaboration, Nucl. Instr. and Meth. A 449 (2000)
394 172.
395 [3] J.B. Birks, The Theory and Practice of Scintillation Counting,
396 Pergamon Press (1964).
397 [4] K. Tolich, Ph.D. dissertation, Stanford University (2008).
398 [5] O. Perevozchikov, Ph.D. dissertation, The University of Ten-
399 nessee, Knoxville (2009).
400 [6] Eljen Technology, EJ-301 data sheet.
401 [7] A.C.L Barnard et al., Nucl. Phys. 86 (1996) 130.
402 [8] P. Dyer et al., Phys. Rev. C 23 (1981) 1865.
403 [9] S. Guldbakke et al., Nucl. Instr. and Meth. A 299 (1990) 367.
404 [10] H.L. Xiao et al., Chin. Phys. C 34 (2010) 571.
405 [11] M.A. Howe et al., IEEE Trans. Nucl. Sci. 51 (2004) 878. URL:
406 <http://orca.physics.unc.edu>
407 [12] A.K. Tripathi et al., Nucl. Instr. and Meth. A 497 (2003) 331.
408 [13] Berger et al., ESTAR, PSTAR, and ASTAR: Computer Pro-
409 grams for Calculating Stopping-Power and Range Tables for
410 Electrons, Protons, and Helium Ions (version 1.2.3). Na-
411 tional Institute of Standards and Technology, Gaithersburg, MD
412 (2005).
413 [14] H. Wan Chan Tseung and N. Tolich, submitted to Phys. Scr.